Chinese Chemical Letters 34 (2023) 108013

Contents lists available at ScienceDirect

Chinese Chemical Letters

journal homepage: www.elsevier.com/locate/cclet

Intermetallic CuAu nanoalloy for stable electrochemical CO_2 reduction

Siyu Kuang[a,1], Minglu Li[a,1], Xiaoyi Chen[a], Haoyuan Chi[a], Jianlong Lin[a], Zheng Hu[d], Shi Hu[d], Sheng Zhang[a,b,c,*], Xinbin Ma[a,b,c]

[a] Key Laboratory for Green Chemical Technology of Ministry of Education, School of Chemical Engineering and Technology, Tianjin University, Tianjin 300072, China
[b] Haihe Laboratory of Sustainable Chemical Transformations, Tianjin 300192, China
[c] Joint School of National University of Singapore and Tianjin University, International Campus of Tianjin University, Fuzhou 350207, China
[d] Tianjin Key Laboratory of Molecular Optoelectronic Science, School of Science, Tianjin University, Tianjin 300072, China

ARTICLE INFO

Article history:
Received 8 August 2022
Revised 4 November 2022
Accepted 20 November 2022
Available online 23 November 2022

Keywords:
CO_2 reduction
CuAu nanoalloy
Intermetallic
Stability
Electrocatalysts

ABSTRACT

Copper is one of the most efficient catalysts widely investigated in electrochemical CO_2 reduction, however, the further development of copper-based catalysts is constrained by severe stability problems. In this work, we developed a method for the synthesis of highly ordered CuAu intermetallic nanoalloys (o-CuAu) under mild conditions (< 250 °C), which can convert carbon dioxide to carbon monoxide with high selectivity and can operate stably for 160 h without current decay. The improved stability is believed to be due to the increased mixing enthalpy and stronger atomic interactions between Cu and Au atoms in the intermetallic nanoalloy. In addition, XPS results, Tafel slope and *in situ* IR spectroscopy demonstrate that high valence gold atoms on o-CuAu surface promote the reduction of CO_2. In contrast, the disordered CuAu nanoalloy (d-CuAu) underwent atomic rearrangement to form a Cu-rich structure on the surface, leading to reduced stability. These findings may provide insight into the rational design of stable CO_2RR electrocatalysts through proper structural engineering.

In recent years, turning greenhouse gas CO_2 into chemical fuels and other energy-intensive products by electrochemical reduction of CO_2 reactions (CO_2RR) has become one of the most promising and challenging topics due to their potential to mitigate emissions and achieve carbon neutrality [1–3]. Copper is one of the most efficient metallic catalysts that can electro-convert CO_2 into hydrocarbons and alcohols with decent efficiencies [2,4,5]. Great efforts have been made to improve the activity and selectivity of Cu-based CO_2RR catalysts in recent years [6–8]. However, copper-based catalysts tend to suffer from more severe stability problems because Cu is a reactive metal that will undergo structural reconfiguration during the CO_2RR process [9,10], which however receives less research attention [11].

To date, some attempts have been made to improve the stability of Cu-based catalysts [12–17]. For example, converting disordered alloy phases into ordered intermetallic compounds is an attractive strategy for improving catalyst stability in fuel cells and water splitting [18–21]. Compared to disordered structures, ordered intermetallic nanoalloys exhibit higher mixing enthalpy and stronger atomic interaction, which help suppress the restructuring of catalyst during reaction and thus improve the stability [22–25]. Yang *et al.* [26] synthesized ordered CuAu nanoparticles as an active catalyst for reducing CO_2 to CO, the high activity was granted from the compressively strained three-atoms-thick gold overlayers. In another research, controlling the amount of Au in the precursor enabled the prepared intermetallic Au_3Cu nanoparticles (NPs) to highly selectively for the CH_4 formation during CO_2RR [27]. Birhanu *et al.* demonstrated that CuAu alloy with an Au-rich surface is more selective towards CO production while the Cu-rich surface favors producing formate [28]. Although ordered intermetallic catalysts can improve stability, the common methods for synthesizing ordered intermetallic materials often require high temperatures (≥ 500 °C) [29–33]. The harsh preparation conditions constrain the further development of ordered intermetallic catalysts [20]. Therefore, it is necessary to develop a mild and low-energy-consuming strategy to synthesize ordered intermetallic NPs and investigate the stability contribution they made in the CO_2RR process.

In this work, we developed a method to prepare CuAu intermetallic materials with atomically ordered arrangements at

* Corresponding author at: Key Laboratory for Green Chemical Technology of Ministry of Education, School of Chemical Engineering and Technology, Tianjin University, Tianjin 300072, China.
E-mail address: sheng.zhang@tju.edu.cn (S. Zhang).
[1] These authors contributed equally to this work.

https://doi.org/10.1016/j.cclet.2022.108013
1001-8417/

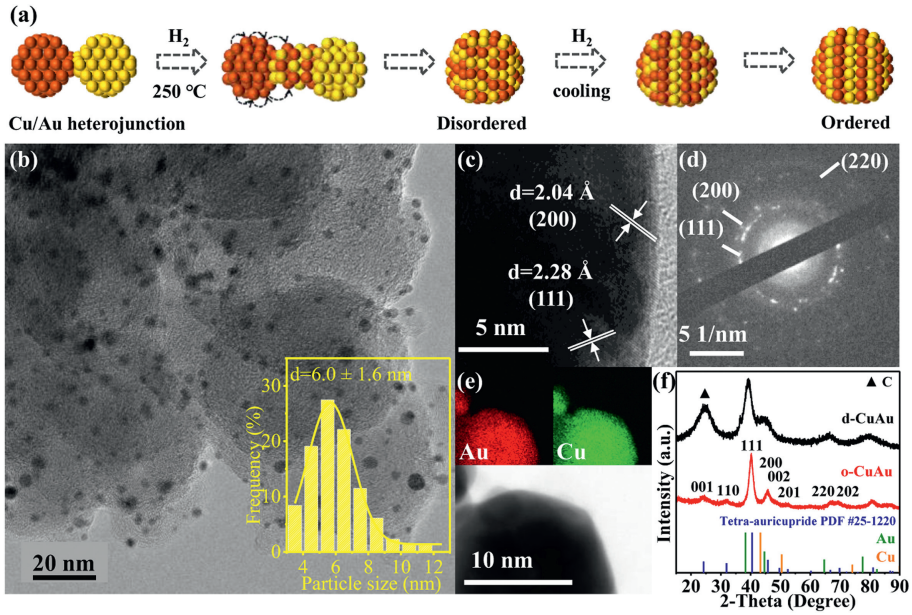

Fig. 1. (a) Schematic illustration of the fabrication of ordered CuAu nanoparticle. (b) TEM image and particle size distribution (PSD) histogram (the inset), (c) HRTEM image, (d) selected area electron diffraction (SAED) image, and (e) HHADF-STEM image and the corresponding EDS elemental (Au, Cu) mappings of CuAu alloy NPs with ordered atomic arrangement (o-CuAu). (f) The XRD patterns of o-CuAu and d-CuAu (CuAu alloy NPs with disordered atomic arrangement).

relatively low temperatures (250 °C). The ordered intermetallic CuAu NPs (o-CuAu) can selectively reduce CO_2 to CO and remain stable during long-term CO_2RR operation. In contrast, the disordered CuAu NPs (d-CuAu) undergo atomic rearrangement during the reaction, forming a Cu-rich structure on the surface, vastly reducing CO selectivity and stability. Therefore, ordered atomic arrangements in intermetallic CuAu nanoalloys are essential to stabilize the active sites and explain the enhanced catalytic stability.

As shown in Fig. 1a, CuAu heterojunction precursor was synthesized using a modified electrostatic self-assembly approach reported in our previous studies [34]. The precursor was then calcined at 250 °C under H_2 for 2 h to form intermetallic CuAu nanoalloy. The diffusion rate of unstable Cu atoms is enhanced in CuAu heterojunctions during hydrogen annealing, facilitating the formation of atomically ordered CuAu nanoalloys [35]. Compared with the common thermal annealing method of heating random alloys at high temperatures (above 500 °C), lower thermal energy is required to overcome the energy barrier during the disordered-to-ordered transition [36]. Fig. 1b showed the TEM image of CuAu alloy NPs presented a nearly monodispersed nanoparticle with ordered atomic arrangement (o-CuAu). The high resolution transmission electron microscope (HRTEM) image showed in Fig. 1c showed two sets of definite lattice fringes with the interplanar spacing of 2.04 and 2.28 Å, corresponding to the (200) and (111) planes in o-CuAu. Moreover, the selected area electron diffraction (SAED) image in Fig. 1d revealed the polycrystalline nature of the o-CuAu NPs with three clear bright rings, which are attributed to (111), (200) and (220) planes of the o-CuAu NPs, which consistent with the HRTEM results. Scanning transmission electron microscopy (STEM-EDS) element mapping result demonstrated that Au and Cu were uniformly distributed in the o-CuAu nanoalloys (Fig. 1e). X-ray diffraction (XRD) patterns were shown for o-CuAu and d-CuAu samples (CuAu alloy NPs with disordered atomic arrangement) in Fig. 1f, where the peak positions of (111) and (200) diffractions in the two CuAu NPs lie between those of pure Au and Cu, which further confirmed the formation of bimetallic system. In particular, the superlattice peaks appeared in o-CuAu and peak splitting at the (200) and (220), indicating that the crystal structure was changed from FCC to body centered tetragonal (Fig. S2a in Supporting information), which indicated atomic ordering in o-CuAu.

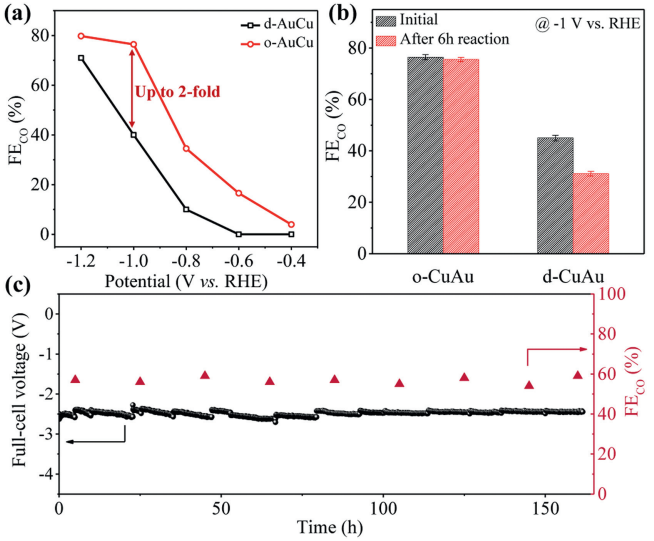

Fig. 2. (a) The faradaic efficiencies (%) of CO (FE_{CO}) of o-CuAu and d-CuAu in 0.1 mol/L CO_2-saturated $KHCO_3$ aqueous solution, at various applied potentials during CO_2RR. (b) Initial FE_{CO} (black) and FE_{CO} after 6 h reaction (red) of o-CuAu and d-CuAu at −1 V *vs.* RHE in 0.1 mol/L CO_2-saturated $KHCO_3$ aqueous solution. (c) 160 h measurement of o-CuAu using a 1 cm^2 MEA electrolyser at a total current density of 100 mA/cm^2 in 0.1 mol/L KOH with fresh electrolyte inject every 5 h.

Electrochemical CO_2 reduction was performed to study the activity of CuAu NPs with different atomic ordering degrees. As shown in Fig. 2a, the faradaic efficiency (FE) of CO over o-CuAu is higher than d-CuAu within the whole potential range with a maximum two-fold increase at −1 V. Notably, the FE_{CO} on o-CuAu can be well maintained after 6 h operation, while the FE_{CO} on d-CuAu decreases significantly (~30%) (Fig. 2b). In addition, the o-CuAu catalyst was loaded in a two-electrode membrane electrode assembly (MEA) device with an effective area of 1 cm^2 for stability testing, and the results showed that o-CuAu exhibited excellent

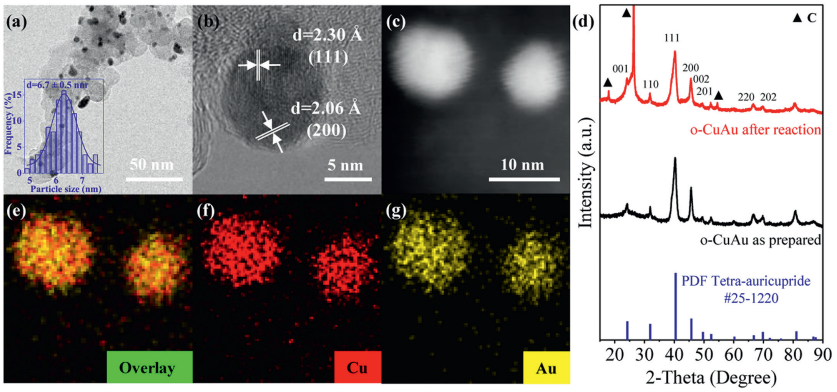

Fig. 3. (a) TEM image and particle size distribution (PSD) histogram (the inset), (b) HRTEM image, (c) HHADF-STEM image and (e-g) the corresponding EDS elemental (Au, Cu) mappings of o-CuAu after 6 h reaction at −1 V *vs.* RHE. (d) The XRD patterns of o-CuAu before and after reaction.

CO_2RR operational stability, capable of stable operation for 160 h without decay at a current density of 100 mA/cm^2, with an applied full-cell voltage of −2.5 V ± 0.2 V and a stable CO FE of ~60% (Fig. 2c).

To further investigate the effect of ordering degree on the catalytic performance, a series of CuAu alloy catalysts with different atomic ordering degrees were prepared by adjusting synthesis temperature. As shown in Fig. S2a, superlattice peaks became more evident and peak splitting of (200) and (220) became more precise for samples synthesized at higher temperatures, indicating the increase in atomic ordering degree of CuAu NPs. Moreover, the long-range order parameter (S) was estimated by the relative intensity ratio of the superlattice peak to the base peak [26]. The o-CuAu synthesized at 250 °C under H_2 had the highest S value of 0.784, accounting for about 89% of atoms in the ordered lattice positions. The intermetallic o-CuAu with high atomic ordering degree (~89%) could be obtained at such low temperature (250 °C), which proves the superiority of the synthesis method. In addition, the purity of reducing atmosphere also had an impact on the atomic arrangement order of CuAu NPs ($S_{o\text{-}CuAu} = 0.784$ for sample synthesized at 250 °C under H_2, while $S_{2\text{-}CuAu} = 0.623$ for synthesized at 250 °C under H_2/Ar) (Fig. S3 in Supporting information).

We further investigated the CO_2RR performance of those intermetallic CuAu nanoalloys with different atomic ordering degrees. It can be seen from Fig. S2b (Supporting information) that initial FE_{CO} increased with the rising atomic ordering degree of CuAu nanoalloys. After 6 h reaction, the intermetallic CuAu samples with a higher atomic ordering degree can retain more of the initial CO selectivity. Zhao *et al.* reported that the ordered arrangement of atoms in intermetallic structures would stabilize the active sites and improve reaction stability [22]. To understand the robust CO_2RR stability of o-CuAu, further characterization of o-CuAu and d-CuAu after the reaction was carried out and shown in Fig. 3 and Fig. S4 (Supporting information). The EDS element mapping of o-CuAu after 6 h reaction at −1 V *vs.* RHE (Figs. 3e-g) demonstrated that Au and Cu were still uniformly distributed. Moreover, the XRD pattern of o-CuAu after reaction showed that the superlattice peaks were still evident, indicating the maintained atomic ordering arrangement after reaction (Fig. 3d). In contrast, the EDS element mapping of d-CuAu after reaction showed that the structure of d-CuAu changed from a well-mixed alloy (before reaction, Figs. S1c-e) to a Cu rich surface and Au rich bulk (Figs. S4e-g). Furthermore, a clear shift of major peak toward monometallic Au has observed in X-ray diffraction (XRD) patterns of d-CuAu after reaction (Fig. S4d), which means that the structure of d-CuAu post-reaction

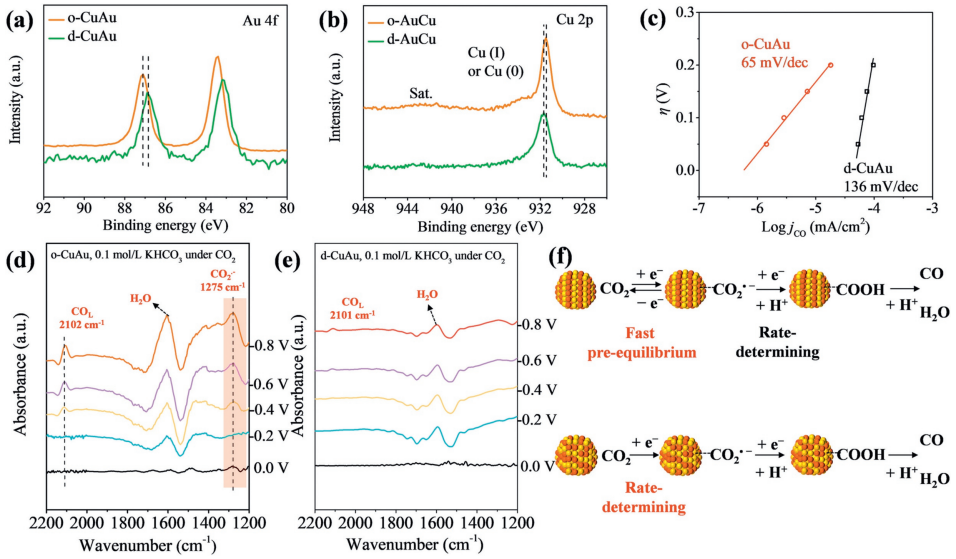

Fig. 4. High-resolution spectra of Au 4f (a) and Cu 2p (b) of o-CuAu and d-CuAu. (c) Tafel plots for production of CO. (d, e) Potential-dependent, attenuated total reflection infrared (ATR-IR) spectra on o-CuAu and d-CuAu in CO_2 saturated 0.1 mol/L $KHCO_3$ from 0.0 V to −0.8 V *vs.* RHE. (f) Proposed mechanisms for CO_2 reduction to CO on o-CuAu and d-CuAu.

is Au enriched in bulk and Cu enriched in surface, consisting with EDS mapping results. The structural evolution of d-CuAu leads to a decrease in FE_{CO}. These results prove the importance of ordered atomic arrangement in improving the stability of the catalyst due to its higher enthalpy of mixing and stronger atomic interaction [28].

XPS characterization was used to identify the chemical state of o-CuAu and d-CuAu. As shown in Fig. 4a, the binding energy of the Au 4f peaks in o-CuAu were shifted appreciably to higher values and the Cu 2p peak also appears to be negatively shifted in comparison with those in d-CuAu (Fig. 4b). The Tafel slope for CO production on o-CuAu is 65 mV/dec, which leads to the mechanism involving a reversible transfer of one electron to CO_2 to form $CO_2^{\bullet-}$ before a chemical rate-determining step [37–39]. The Tafel slope of 136 mV/dec on d-CuAu indicates a rate-determining initial electron transfer to form an adsorbed $CO_2^{\bullet-}$ intermediate (Fig. 4c), a step which overpotential is typically large at metal electrodes due to the poor stability of the metal surface to $CO_2^{\bullet-}$. To further investigate the CO_2RR mechanism of o-CuAu and d-CuAu, we performed *in situ* attenuated total reflection infrared (ATR-IR) spectroelectrochemical measurements to monitor the key reaction intermediate ($CO_2^{\bullet-}$). As shown in Fig. 4d, the vibration bands at approximately 1275 cm^{-1} are assigned to the characteristic vibration adsorption of $CO_2^{\bullet-}$ on o-CuAu and no such band was observed on d-CuAu (Fig. 4e), which is aligned with the mechanisms of 1 electron pre-equilibrium on o-CuAu and rate-determining 1 electron transfer on d-CuAu supported by the electrokinetic data. The results were summarized in Fig. 4f, which is consistent with previous report that Au particles with high valence can accelerate CO_2 reduction to CO [39].

In summary, this work provides a mild method to prepare highly ordered CuAu intermetallic (o-CuAu), the acquired atomic ordering arrangement could greatly affect their performance towards electrochemical CO_2 reduction. The d-CuAu underwent atomic rearrangement during the reaction, and formed a structure with Cu rich surface, which exhibited poor CO selectivity and stability during long-term CO_2RR. In contrast, due to the high mixing enthalpy and strong atomic interactions between Cu and Au atoms, o-CuAu selectively converted CO_2 to CO and demonstrated excellent stability. Those results suggest that the ordered atomic arrangement plays an essential role in improving the stability of bimetallic catalysts, which will provide guidelines for designing efficient electrocatalysts.

Declaration of competing interest

The authors declare that they have no known competing financial interests or personal relationships that could have appeared to influence the work reported in this paper.

Acknowledgments

The authors are grateful for the financial support from National Nature Science Foundation of China (Nos. 22078232 and 21938008), and the Science and Technology Major Project of Tianjin (Nos. 19ZXNCGX00030 and 20JCYBJC00870).

Supplementary materials

Supplementary material associated with this article can be found, in the online version, at doi:10.1016/j.cclet.2022.108013.

References

[1] Q. Lu, F. Jiao, Nano Energy 29 (2016) 439–456.
[2] F. Wang, W. Zhang, H. Wan, et al., Chin. Chem. Lett. 33 (2022) 2259–2269.
[3] S. Nitopi, E. Bertheussen, S.B. Scott, et al., Chem. Rev. 119 (2019) 7610–7672.
[4] H. Zhang, C. He, S. Han, et al., Chin. Chem. Lett. 33 (2022) 3641–3649.
[5] M. Gattrell, N. Gupta, A. Co, Chemistry 594 (2006) 1–19.
[6] S. Kuang, M. Li, R. Xia, et al., ACS Appl. Nano Mater. 3 (2020) 8328–8334.
[7] L. Zhang, Q. Fan, K. Li, et al., Sustain. Energy Fuels 4 (2020) 5417–5432.
[8] S. Zhang, H. Liu, N. Zhang, et al., Chin. J. Catal. 40 (2019) 1904–1911.
[9] C.T. Dinh, T. Burdyny, M.G. Kibria, et al., Science 360 (2018) 783–787.
[10] C.W. Li, M.W. Kanan, J. Am. Chem. Soc. 134 (2012) 7231–7234.
[11] S. Popović, M. Smiljanić, P. Jovanovič, et al., Angew. Chem. 132 (2020) 14844–14854.
[12] Z. Xin, Z. Yuan, J. Liu, et al., Chin. Chem. Lett. 34 (2023) 107458.
[13] S. Zhang, Q. Fan, R. Xia, et al., Acc. Chem. Res. 53 (2020) 255–264.
[14] R. Xia, S. Zhang, X. Ma, et al., J. Mater. Chem. A 8 (2020) 15884–15890.
[15] S. Zhang, P. Kang, M. Bakir, et al., Proc. Natl. Acad. Sci. U. S. A. 112 (2015) 15809–15814.
[16] S. Zhang, P. Kang, T.J. Meyer, J. Am. Chem. Soc. 136 (2014) 1734–1737.
[17] S. Kuang, M. Li, R. Xia, et al., ACS Appl. Nano Mater. 3 (2020) 8328–8334.
[18] J. Liang, F. Ma, S. Hwang, et al., Joule 3 (2019) 956–991.
[19] J.T. Gamler, H.M. Ashberry, S.E. Skrabalak, et al., Adv. Mater. 30 (2018) 1801563.
[20] Y. Yan, J.S. Du, K.D. Gilroy, et al., Adv. Mater. 29 (2017) 1605997.
[21] H.M. Ashberry, J.T. Gamler, R.R. Unocic, et al., Nano Lett. 19 (2019) 6418–6423.
[22] T. Zhao, G. Wang, M. Gong, et al., ACS Catal. 10 (2020) 15207–15216.
[23] J. Li, Z. Xi, Y. Pan, et al., J. Am. Chem. Soc. 140 (2018) 2926–2932.
[24] J. Li, S. Sharma, X. Liu, et al., Joule 3 (2019) 124–135.
[25] L. Luo, M. Wang, Y. Cui, et al., Angew. Chem. 132 (2020) 14542–14550.
[26] D. Kim, C. Xie, N. Becknell, et al., J. Am. Chem. Soc. 139 (2017) 8329–8336.
[27] W. Zhao, L. Yang, Y. Yin, et al., J. Mater. Chem. A 2 (2014) 902–906.
[28] M.K. Birhanu, M.C. Tsai, C.T. Chen, et al., Electrochim. Acta 356 (2020) 136756.
[29] L. Du, S. Zhang, G. Chen, et al., ACS Appl. Mater. Interfaces 6 (2014) 14043–14049.
[30] S. Ma, M. Sadakiyo, M. Heima, et al., J. Am. Chem. Soc. 139 (2017) 47–50.
[31] S. Zhu, X. Qin, Q. Wang, et al., J. Mater. Chem. A 7 (2019) 16954–16961.
[32] P. Wang, M. Qiao, Q. Shao, et al., Nat. Commun. 9 (2018) 4933.
[33] J. Wang, Y. Ji, Q. Shao, et al., Nano Energy 59 (2019) 138–145.
[34] S. Zhang, Y. Shao, G. Yin, et al., Angew. Chem. Int. Ed. 49 (2010) 2211–2214.
[35] G. Battaglin, E. Cattaruzza, F. Gonella, et al., Nucl. Instrum. Methods Phys. Res. 166 (2000) 857–863.
[36] H. Kim, S. Joo, J. Mater. Chem. A 8 (2020) 8195.
[37] Y. Chen, M.W. Kanan, J. Am. Chem. Soc. 134 (2012) 1986–1989.
[38] E. Gileadi, Electrode Kinetics for Chemists, Chemical Engineers, and Material Scientists, Wiley Publishers, New York, 1993.
[39] Y. Chen, C.W. Li, M.W. Kanan, J. Am. Chem. Soc. 134 (2012) 19969–19972.